12 Moisture budget equation and application to Sahel Drought

a) de Groot and Mazur, Non-Equilibrium Thermodynamics, Dover Publications, Inc., New York, 501 pp.

b) Charney, J.G., 1975: Dynamics of deserts and drought in Sahel. *Q J Roy Meteorol Soc*, **101**, 193–202

c) Zeng N., Neelin J.D., Lau K.-M., Tucker C.J., 1999: 'Enhancement of interdecadal climate variability in the Sahel by vegetation interaction. *Science*, **286**, 1537-1540

d) Xue, Y., et al., 2016: 'West African monsoon decadal variability and surface-related forcings: second West African Monsoon Modeling and Evaluation Project Experiment (WAMME II).' *Climate Dynamics*, **47**, 3517-3545.

e) Kucharski, F., Zeng, N., Kalnay E., 2012: A further assessment of vegetation feedback on decadal Sahel rainfall variability. *Climate Dyn.*, DOI:10.1007/s00382-012-1397-x

Let us consider the general equation for conservation of the water mass in an infinitesimal volume of air (de Groot and Mazur)

$$\rho \frac{dm_v}{dt} = -\nabla \cdot \mathbf{F_{m_v}} - S_{m_v} \ , \tag{265}$$

where m_v is the mass fraction of water vapour $m_v = \rho_v/\rho$ (or specific humidity), $\mathbf{F_{m_v}}$ is the diffusive water vapour flux, and S_{m_v} are the local sinks or sources of water vapour (e.g. local precipitation, or evaporation in the air). A typical near-surface specific humidity distribution is shown in Fig. 57. Discuss the distribution! Why do we see maximum values in some specific regions?

Using the continuity equation 135, Eq. 265 can be reformulated as (Exercise!)

$$\frac{\partial \rho_v}{\partial t} = -\nabla \cdot (\rho_v \mathbf{v} + \mathbf{F_{m_v}}) - S_{m_v} \ . \tag{266}$$

If we vertically integrate this equation, we get

$$\frac{\partial \int_0^\infty \rho_v dz}{\partial t} = -\left|\rho_v w\right|_0^\infty - \left|F^z_{m_v}\right|_0^\infty - \int_0^\infty \nabla_h \cdot (\rho_v \mathbf{v}_h + \mathbf{F_{m_v}}) dz - \int_0^\infty S_{m_v} dz \ . \tag{267}$$

The first term on the rhs vanishes, because $w(z=0) = 0$ and $\rho_v(z=\infty) = 0$. Furthermore, assuming $F^z_{m_v}(z=\infty) = 0$, and $F^z_{m_v}(z=0) = E$ (surface evaporation flux), $\int_0^\infty S_{m_v} dz = P$ (precipitation). Assuming further a stationary state (or rate of change in time to be small), as well as the horizontal specific humidity diffusion to be negligible, the vertically integrated moisture budget becomes

$$P = E - \int_0^\infty \nabla_h \cdot (\rho_v \mathbf{v}_h) dz \quad . \tag{268}$$

This is an important equation, which is often used in the analysis of the origin of precipitation. It tells us that any local precipitation must come from either local evaporation or the vertical integrated moisture flux (horizontal) convergence, and obviously we have $P = E$ for global integrals of it. Equation 268 can be further split for a more detailed interpretation

$$P = E - \int_0^\infty (\rho_v \nabla_h \cdot \mathbf{v}_h + \mathbf{v}_h \cdot \nabla_h \rho_v) dz \quad . \tag{269}$$

The first term of the integral may be interpreted in the way that any horizontal convergence (or almost equivalently positive vertical motion, why?) in the presence of moisture will lead to a precipitation increase. This is interesting, because it combines nicely with the fact that a parcel that rises high enough will necessarily reach supersaturation and therefore water vapour will condense. The second term in the integral may be interpreted as moisture advection from wetter regions to dryer regions. This second term is less important that the first one, but plays sometimes also an important role. Note also that often Eq. 268 or 269 are evaluated in pressure coordinates using $\int \rho \psi dz = -\int \psi dp/g$, leading to

$$P = E - \int_0^{ps} \nabla_h \cdot (m_v \mathbf{v}_h) dp/g \quad . \tag{270}$$

Fig. 58 shows the annual mean distribution of evaporation and precipitation. Discuss the important features of these distributions. Where is evaporation maximal and where is precipitation maximal?

12.1 An application to Sahel drought

The Sahel Drought is one of the most important and most studied climatic events in the 20th century. Fig. 59 shows the worlds desert regions and clearly identifies the Sahara as the largest and brightest desert regions.

The Sahel region is the region at the southern edge of the Sahara Desert, and has the characteristics of modest, but highly variable rainfall as indicated by mean rainfall, decadal standard deviation and Coefficient of Variation (Figs 60 and 61a,c).

If we concentrate now on Sahel rainfall (averaged rainfall in the region 15° W to 37.5° E, 12.5° to 17.5° N), then we see striking decadal rainfall variations compared to interannual variations (Fig. 62).

As can be seen from the time series in the 1970s to the 1990s prolonged drought periods have been observed, but a much wetter period in the 1950s and 1960s. An intriguing feature for scientists (but problematic for the Sahel population) is the long duration of the dry periods, with sometimes nearly 10 years of continuous negative or positive anomalies (note that no filtering has been applied to this time series, only in the red smooth curve). As said above, many scientific studies have been performed to address the physical mechanisms for the Sahel drought from the 1970s to the 1990s. A general consensus is now that it is induced by sea surface temperature variations, but enhanced by land-surface feedbacks. Also human-induced land-use

changes and aerosols may have played a role (e.g. Xue et al, 2016 for a review). In order to highlight these decadal changes further, we show in Fig. 63 the rainfall difference 1980 to 1994 minus 1950 to 1964, roughly representing the core periods for dry and wet conditions, respectively. It is seen that the drying is a very large-scale phenomenon, but it can also be seen that there are slightly wet conditions to the south of the Sahel.

Here we will focus on the role that interactive vegetation may have played. In order to assess this we will show some results from the analysis of Kucharski et al. (2012), where the vegetation impact on Sahel rainfall variability has been investigated using an AGCM coupled to a dynamic interactive vegetation model (see Fig. 64).

An equation for the dynamic vegetation may be formulated as (Zeng et al., 1999)

$$\frac{dV}{dt} = a\beta_{veg}(W)(1 - e^{-\kappa L}) - \frac{V}{\tau} \quad , \tag{271}$$

where V is the vegetation cover, a is a coefficient, $\beta_{veg}(W)$ is the soil moisture W dependence of vegetation growth (which could be linear), κ is the extinction coefficient of photosynthesis, L is the leaf area index, τ is the vegetation time scales (set to 1 year; Discuss the solution for small L and $L = 0$). There is assumed also a linear relation between L and V, i.e. $L = L_{max}V$. Obviously, there is also an equation for W, which will tell us essentially that soil moisture will grow when precipitation is large, and so further. For us its important to note the main impact for the atmosphere will be the relation between albedo and vegetation cover (or L), which is parameterized empirically as

$$A = 0.38 - 0.3(1 - e^{-\kappa L}) \tag{272}$$

Between what values varies the albedo (reflectivity) according to this equation? Obviously, with this the vegetation cover modified strongly the atmospheric radiative balance.

The first question that has to be addressed is whether the model can reproduce the mean climate in the regions in terms of rainfall and vegetation. Fig. 60, lower panel, shows the modeled rainfall and LAI climatologies. The model represents at least the gross regional characteristics.

Also the model decadal standard deviation and COV (Fig. 61, b,d) show overall spatial characteristics similar to observations. Does the model reproduce the Sahel drought?

Fig. 65 compares the models response for the Sahel drought rainfall difference when vegetation is interactively coupled and prescribed to be constant. Clearly the interactive vegetation version of the model gives a response that is much closer in magnitude compared the the non-interactive version, even though the overall drought signal is present in both simulations.

Let's investigate the feedback mechnism that the interactive vegetation model can provide for drought/wet conditions. Fig. 66 shows several components of the

positive feedback mechanism involved when dynamic vegetation coupling is present in the response. Panel (a) shows the vegetation cover response, and indicates that there is a reduction in vegetation when the precipitation is reduced (see Eq.271). This is leading to an increase in albedo (surface reflectivity) as shown in panel (b) (see Eq. 272). This means that more solar radiation at the surface is reflected (c). The feedback loop is closed by the impact of the reduced net surface radiation on the circulation. Charney (1975) suggested that the reduced surface net radiation will lead to less surface warming, thus inducing high pressure, Ekman divergence, and sinking motion (e.g. moisture flux divergence according to Eq. 269) and thus reduced rainfall. On the other hand, the model without interactive vegetation cannot produce this feedback (panel d). Fig. 67 summarises the *Charney feedback mechanism*.

We will see however, that the feedback mechanism is slightly more complex than initially suggested by Charney, and involves more components, also non-local feedbacks. Fig. 68a and b shows the moisture flux convergence and the evaporation terms of Eq. 268. As can be seen, in the Sahel region local evaporation plays a substantial role in the moisture budget. However, the moisture flux convergence term plays the dominant role, supporting Charney's hypothesis. The reduced evaporation means, however, that at least part of the reduced surface heating is compensated by reduced surface latent heatflux. Panels b) and d) show the moisture flux convergence and evaporation for the model with fixed vegetation. Both are substantially weaker.

Fig. 69a shows the corresponding surface pressure and low-level wind responses for the Sahel. As hypothesised by Charney there is high pressure and low-level divergent response. However, in particular the high pressure response is shifted to the north, so that the advection of dry air from the Sahara will also contribute to the drying (e.g. second term in the moisture flux convergence of Eq. 269). It can also be noted that the dynamic feedback is much stronger in the case with interactive vegetation compared with the non-interactive vegetation (Fig. 69b).

Finally, we compare the model Sahel rainfall time series with the observed (Fig. 70). Whereas the time series from the interactive vegetation run has characteristics similar to the observed rainfall (but slightly weaker magnitude; Fig. 70b), the model without interactive vegetation (Fig. 70c) has much more power at interannual time scales and less persistent anomalies as well as smaller magnitudes.

Exercises

1. Show with help of the full continuity equation that Eq. 266 follows from Eq. 265.

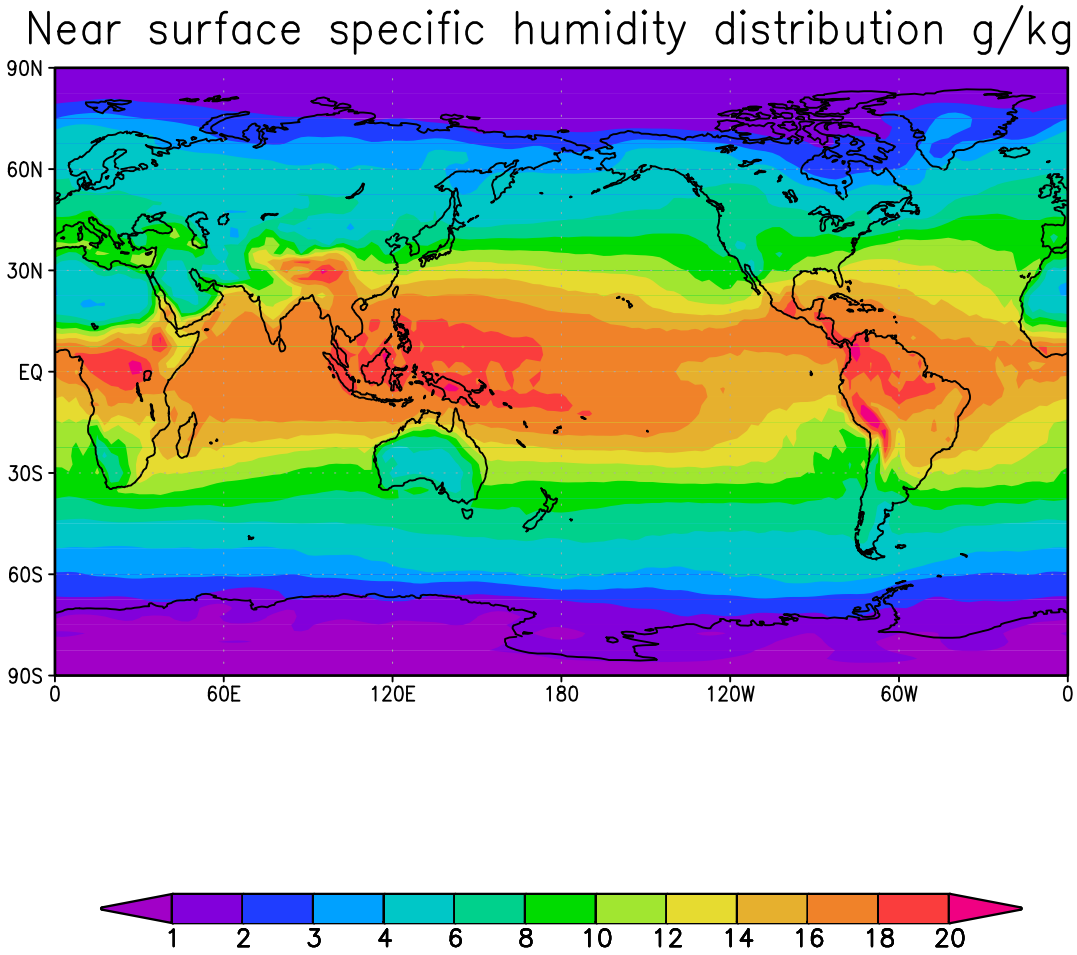

Figure 57: Near surface distribution of specific humidity (vapour mass fraction). Units are g/Kg.

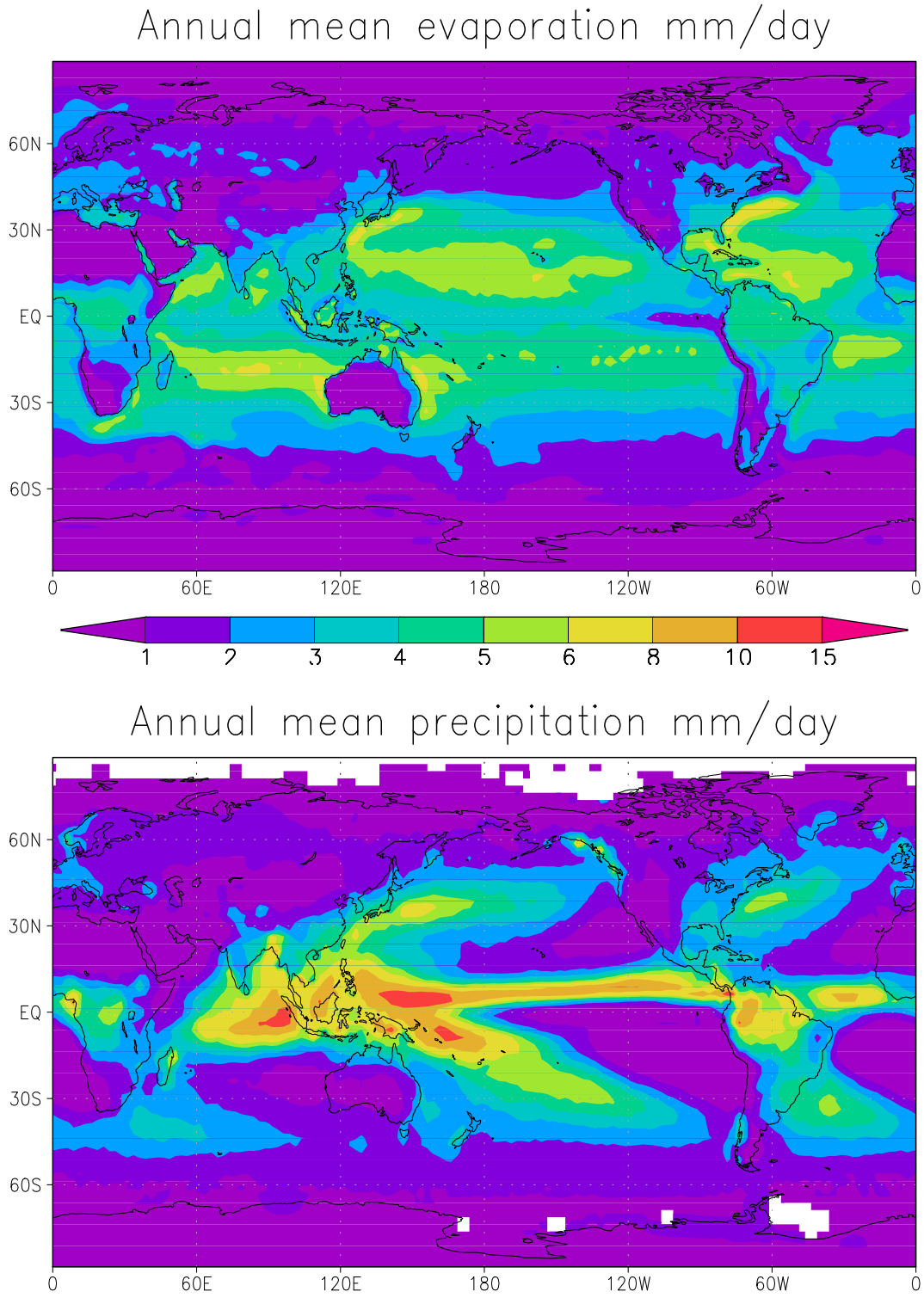

Figure 58: Annual mean observed evaporation (top) and precipitation (bottom).

Figure 59: Vegetations and brightness of the Earth.

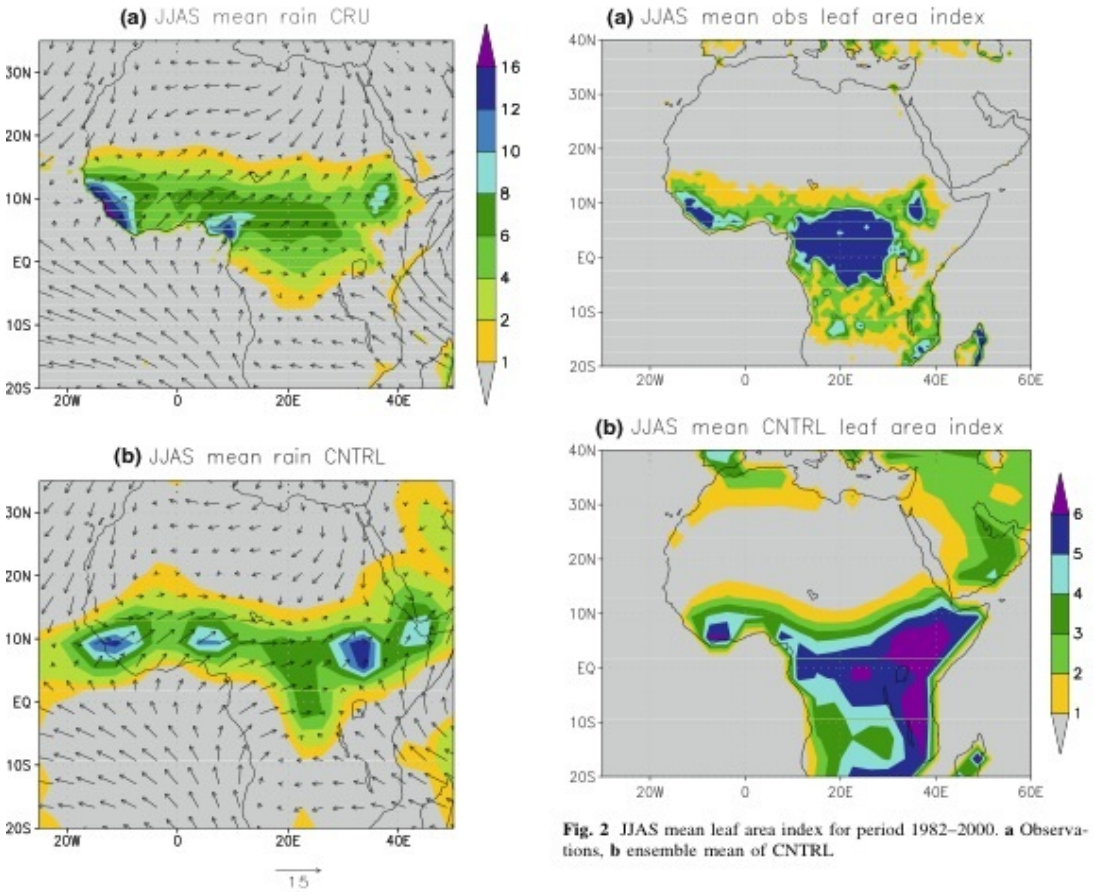

Fig. 2 JJAS mean leaf area index for period 1982–2000. **a** Observations, **b** ensemble mean of CNTRL

Figure 60: Precipitation in mm/day and Leaf Area Index (LAI; leaf area/ground area in m^2/m^2) of observations (upper panel) and model (lower panel).

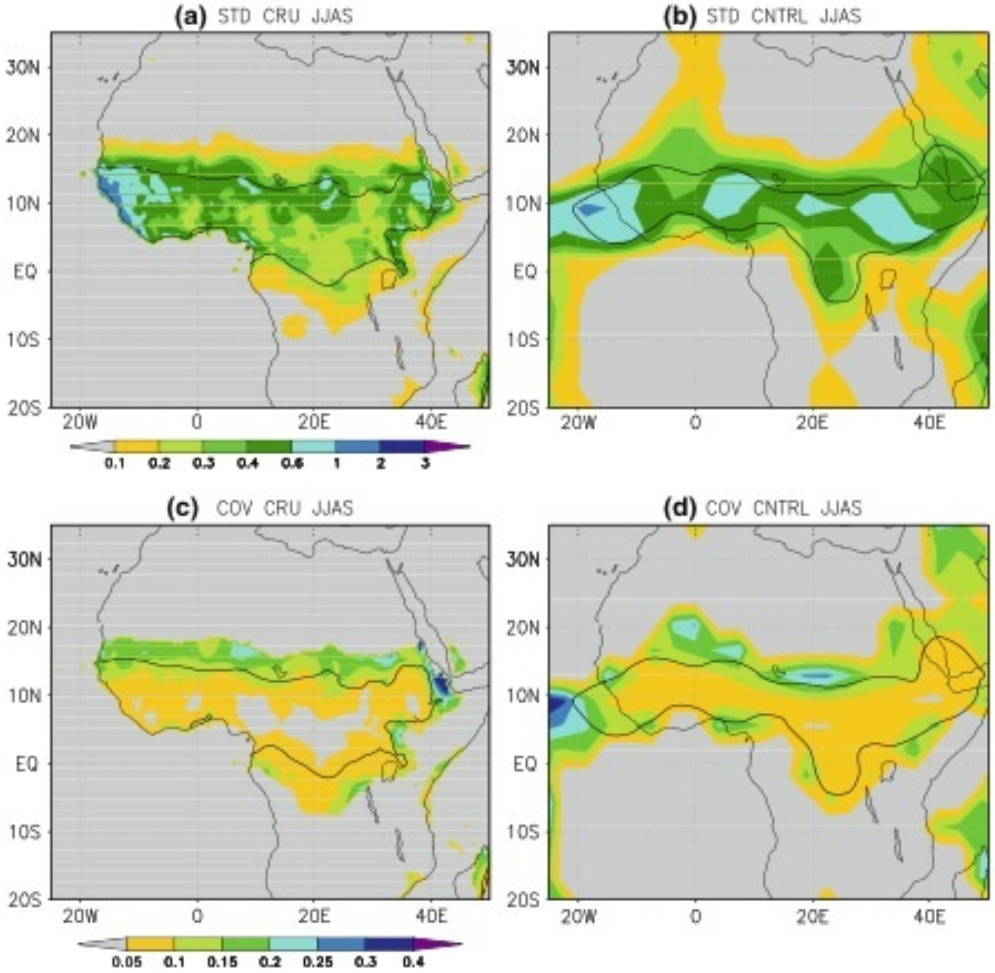

Figure 61: Observed (a, c)and model (b,d) precipitation standard deviations in mm/day and Coefficient of Variation (COV), defined as rainfall standard deviation divided by mean rainfall.

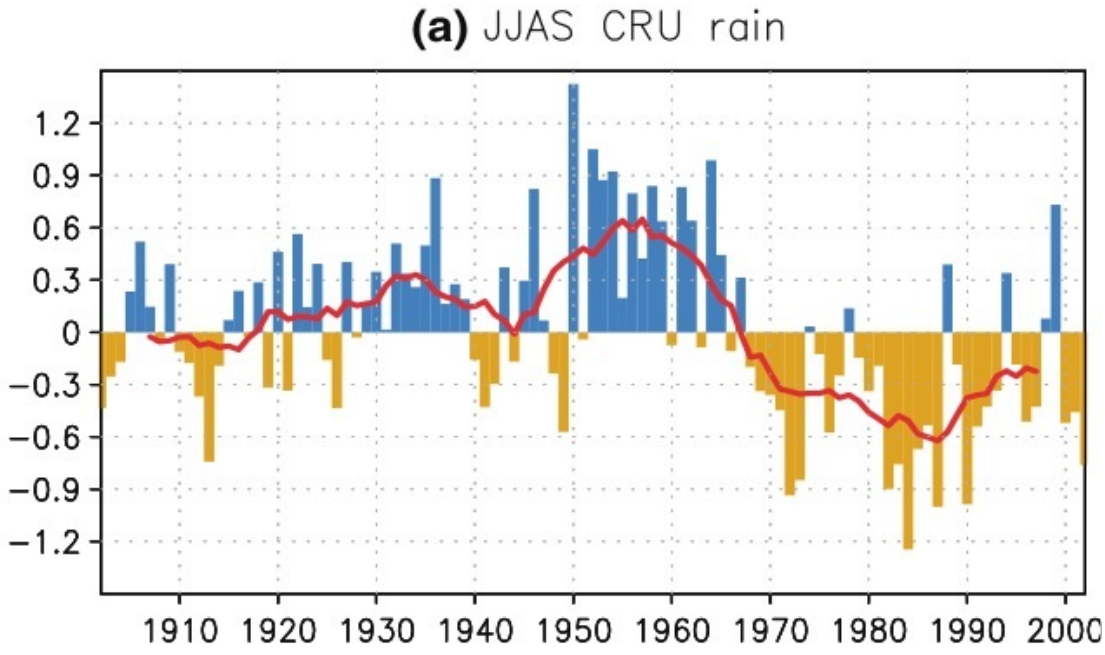

Figure 62: Sahel rainfall anymalies in mm/day.

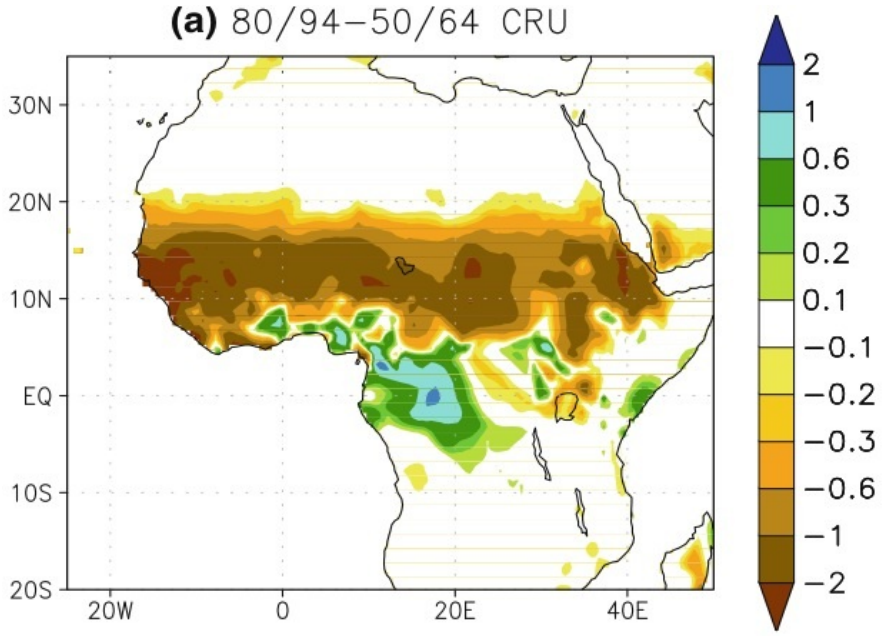

Figure 63: Rainfall difference 1980 to 1994 minus 1950 to 1964 in mm/day.

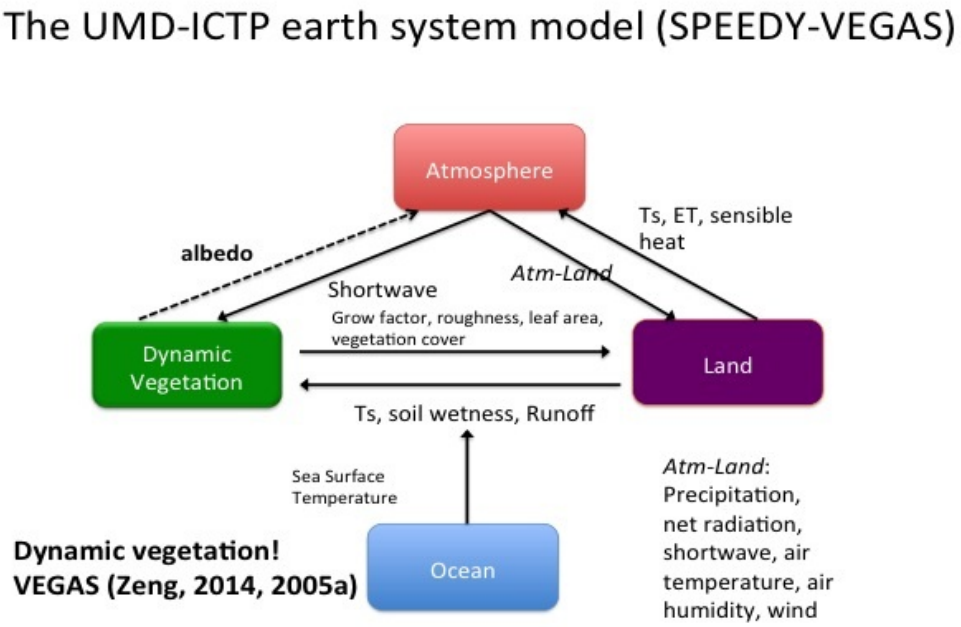

Figure 64: Model set-up.

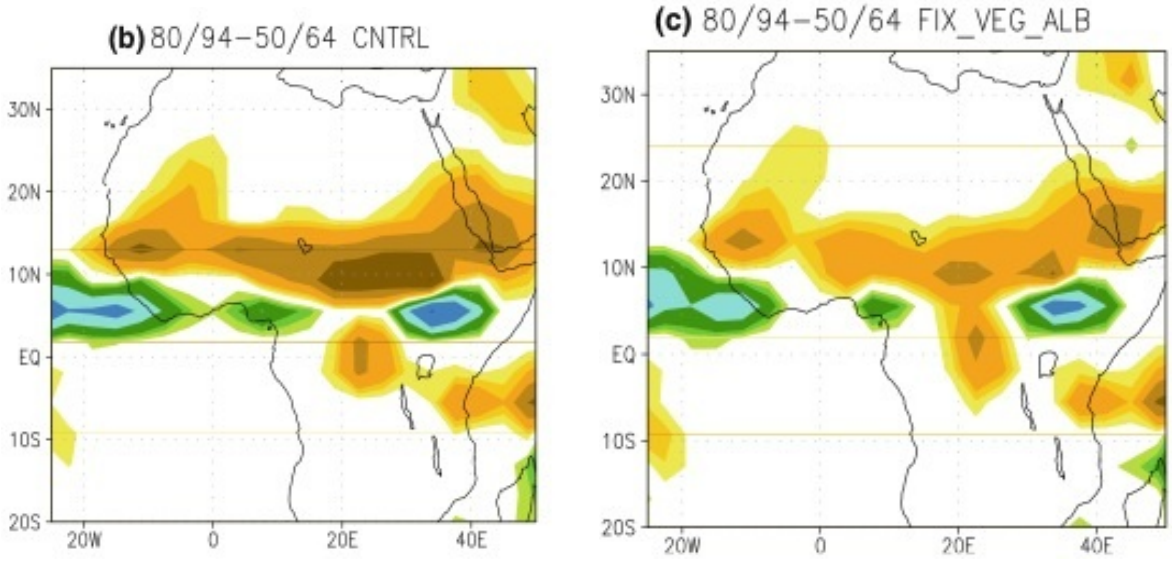

Figure 65: Modeled rainfall difference 1980 to 1994 minus 1950 to 1964 in mm/day. Left: with interactive vegetation, right: without interactive vegetation). of observations and model.

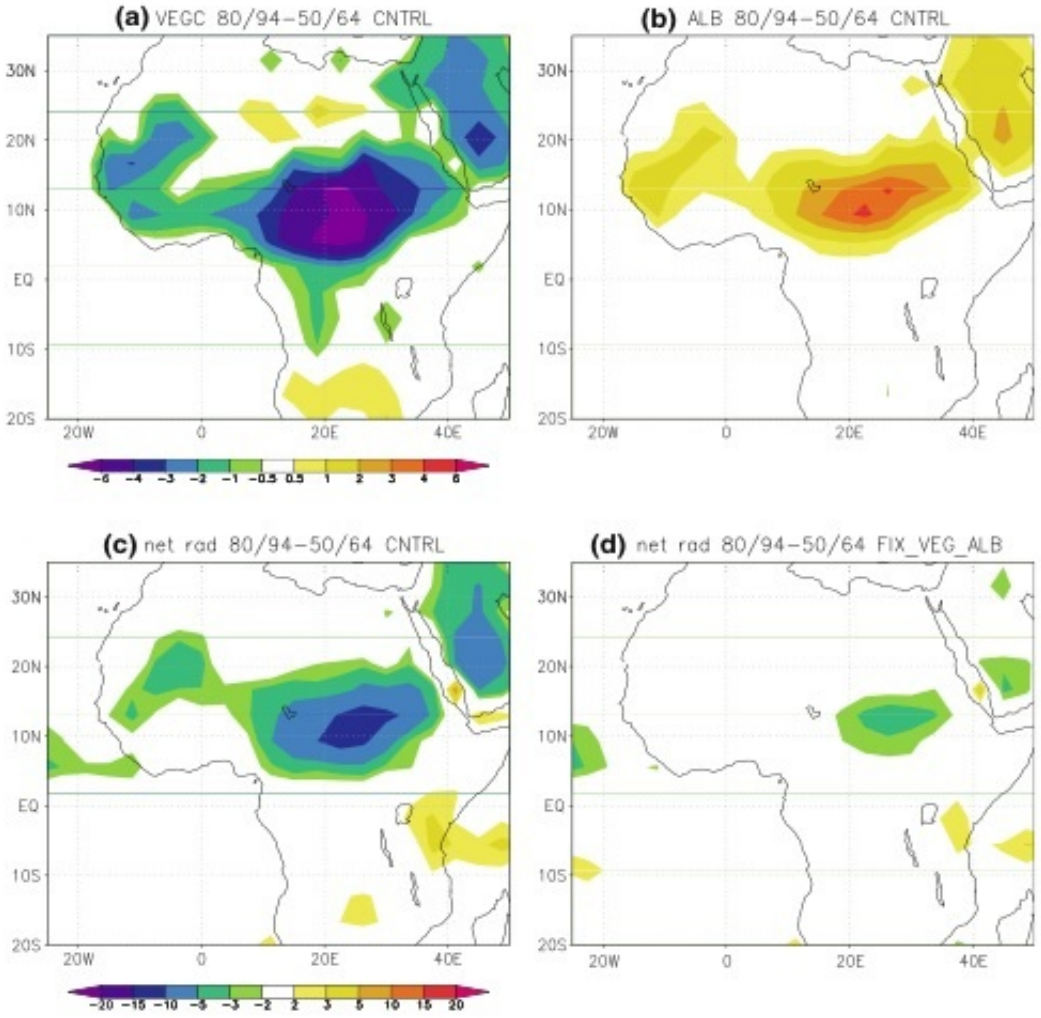

Figure 66: Features of the Charney Feedback mechanism responsible for the responses 1980 to 1994 minus 1950 to 1964 in the model with dynamics vegetation: a) Vegetation cover change [%], b) Albedo change [%], c) net surface radiation change [W/m^2], d) as c) but without vegetation feedback [W/m^2].

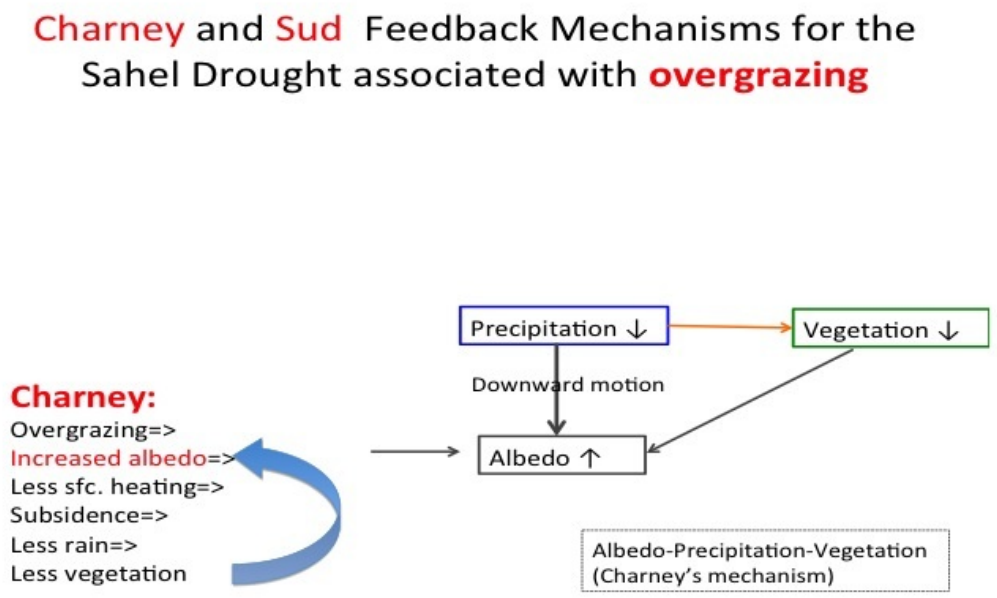

Figure 67: Schematic of the Charney feedback mechanism.

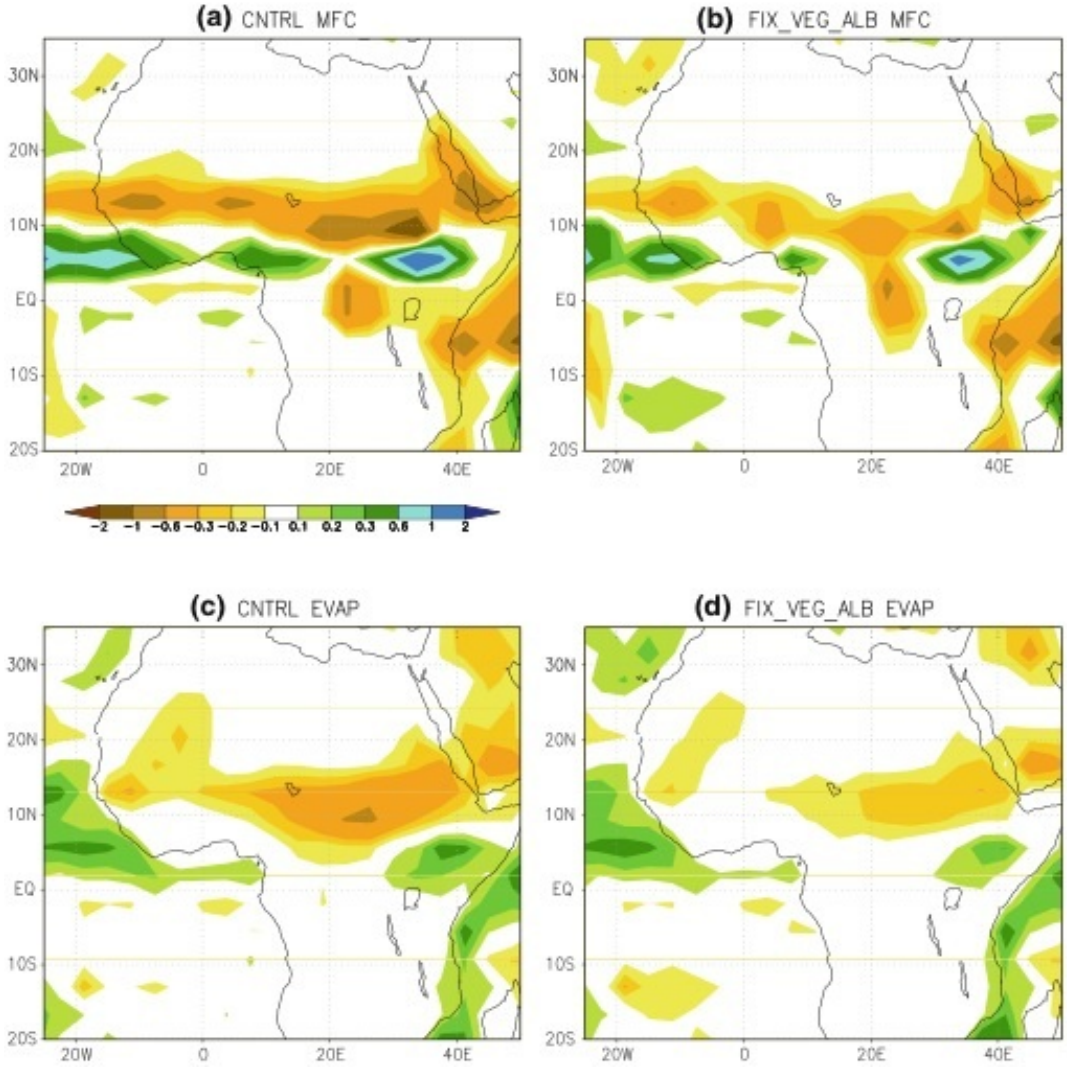

Figure 68: Moisture budget terms in mm/day. a) Moisture flux convergence term of the interactive vegetation, b) moisture flux convergence term of the fixed vegetation model, c) evaporation on the interactive vegetation, d) evaporation of the fixed vegetation

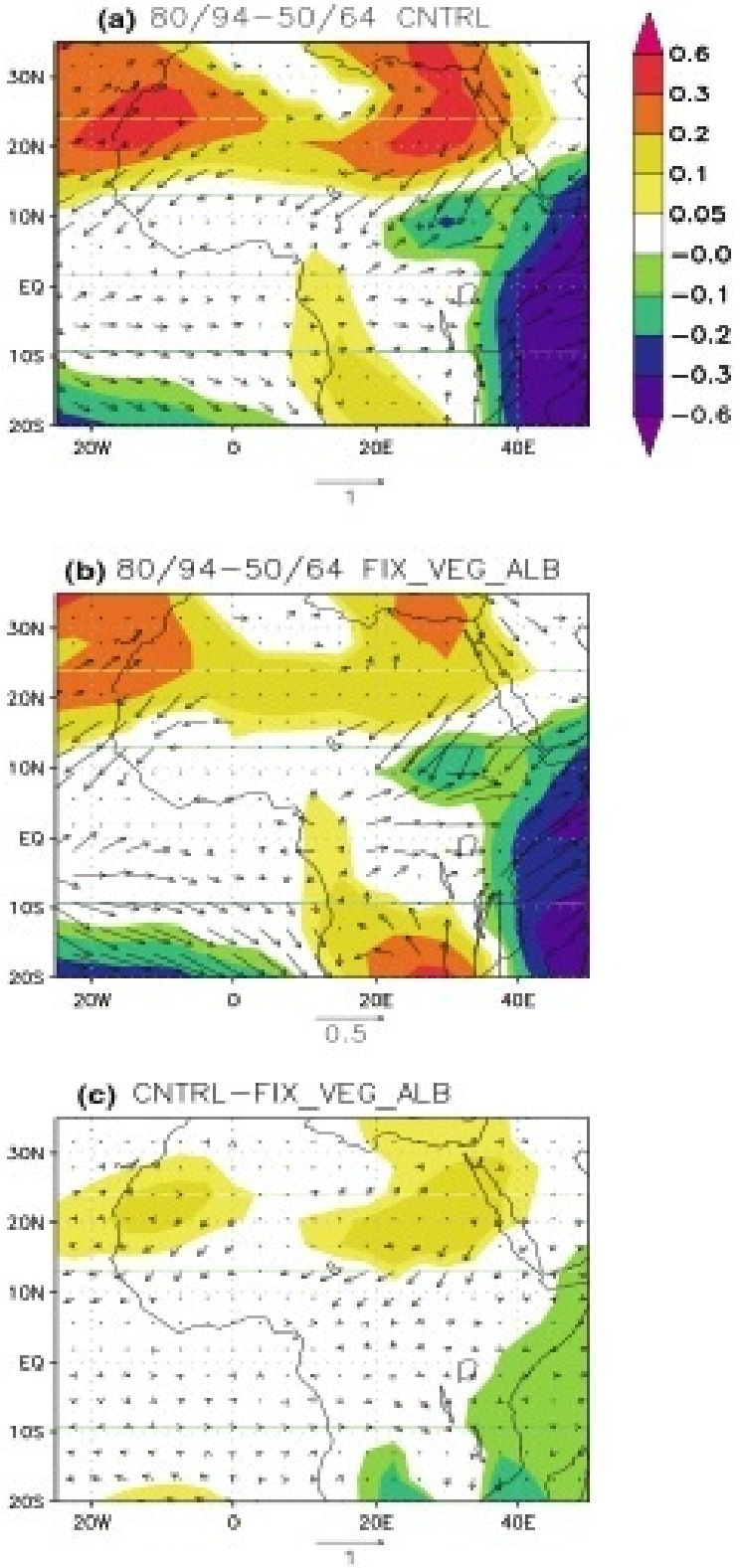

Figure 69: Response of surface pressure [hPa] and low-level winds [m/s] for a) interactive vegetation model, b) non-interactive vegetation model and c) difference

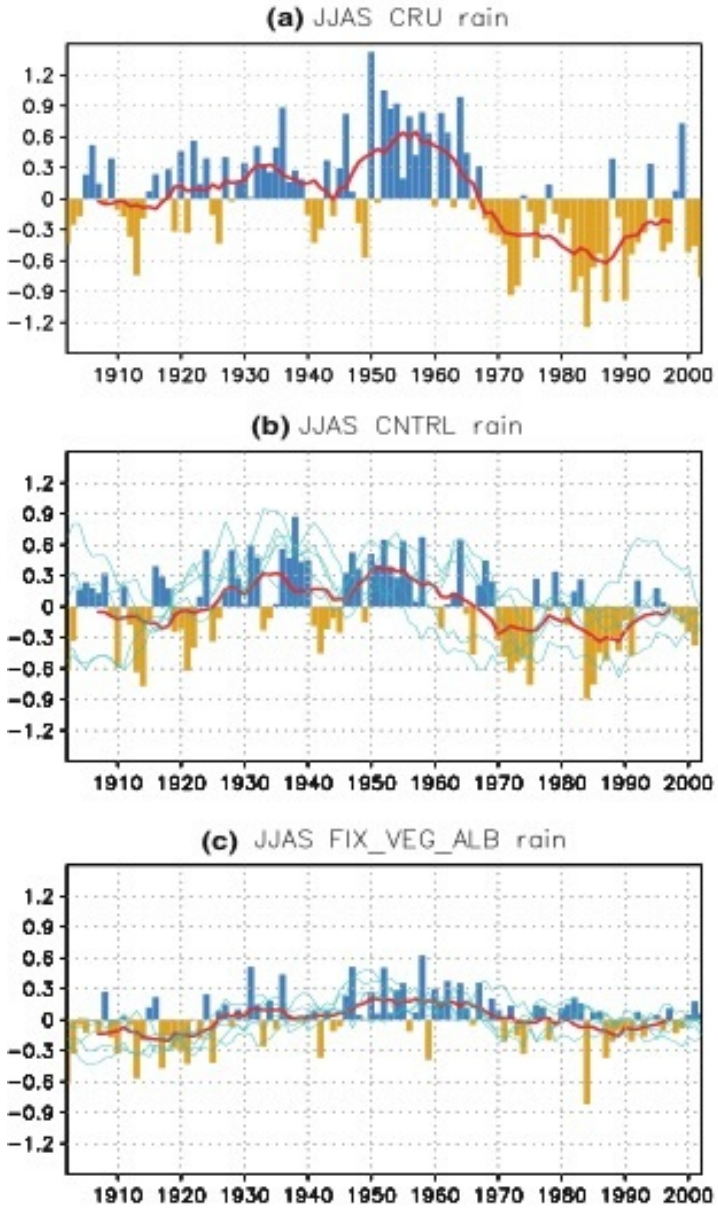

Figure 70: Sahel rainfall anymalies in mm/day. a) Observations, b) model with interactive vegetation, c) model without interactive vegetation.